A novel air reactor concept for chemical looping combustion systems operated at high pressure

J.C. Abanades*, M.E. Diego, J.R. Fernández

Spanish Research Council. CSIC-INCAR, Fco. Pintado Fe 26, 33011 Oviedo, Spain

*abanades@incar.csic.es

Keywords: CO_2 capture, chemical looping combustion, energy storage, backup power, reactor design

Abstract

We analyse the viability of a novel reactor concept for chemical looping combustion applications with CO_2 capture. The reactor consists of a packed bed of reduced oxygen carrier particles traversed by a series of empty conducts oriented in the axial direction. These conducts are made of permeable but non-selective porous walls, through which air diffuses towards the region of reacting solids. The diffusion flux of air through the orifices, which is perpendicular to the main bulk flow of gas along the conducts, imposes very long oxidation times for all the reacting particles and a quasi-steady heating up of the air flow. The conducts designed to have a very high length/diameter ratio (i.e. above 50) allow a large bypass of pressurized air through the reactor without coming into direct contact with the solids, resulting in a modest pressure drop of the gas (i.e. below 5% at the reactor exit). A preliminary reactor design example is described for a case using Fe/Fe_2O_3 pellets as oxygen carrier, which are packed into a reactor (L=100 m, I.D.=2 m) traversed by air conducts (I.D.=0.05 m) with a wall 2 mm thick and orifices occupying an area fraction of 0.12. The reactor can initially generate 100 MW_{th}, with a gas flow at the exit at close to 1050ºC and 19 atm, and it could be used intermittently for more than 9 hours as the main heater in a highly efficient Brayton cycle.

Introduction

Chemical looping combustion (CLC) technology is widely recognised to have potential for CO_2 capture with negligible energy penalties [1-4]. Recent reviews on CLC report on the substantial progress made in recent decades on the development of oxygen carriers, pilot plant operation and process variants [5-15]. For power plant applications using clean fuel gases, high energy conversion efficiencies require the air reactor to operate at high pressures and at the highest possible temperature to avoid functional and/or structural damage to the materials [1, 4, 16-18]. Interconnected fluidized-bed reactors are the main configuration proposed to carry out CLC processes. The efficient mixing of gas and solids in these reactors facilitates the control of the temperature during the fast and energy-intensive redox reactions characteristic of CLC systems [10,15]. However, interconnected fluidized-beds at high pressure still face serious challenges, such as the necessity to maintain a stable solids circulation between the reactors and the need for high-T and high-P filtering devices to remove fine particles from the gas that could otherwise affect the performance of downstream turbines [19,20]. Pressurized packed-bed reactors have been proposed to overcome these limitations. However, they have to deal with high temperature profiles caused by sharp reaction fronts that appear in the bed [21-25]. Different heat management strategies have been investigated to control the fluctuations in temperature, especially during the highly-exothermic oxidation stage of CLC systems. One alternative is to use oxygen carriers with low active phase contents. The heat released during the oxidation reaction is then absorbed by a large amount of inert solid, thereby moderating the temperature in the reaction front, but at the expense of having to use larger reactors for a given fuel input [26,27]. Packed-bed reactors loaded with high proportion of active oxygen carrier can be operated by recirculating a fraction of the product gas. The dilution of the gaseous feed allows the displacement of both reaction and heat transfer fronts to be controlled along the bed without exceeding the temperature limits. A configuration of this type allows more compact reactor designs but it involves greater energy demand and higher equipment cost because of the large gas recirculation [28,29]. CLC packed-bed reactors can also be operated by periodically reversing the direction of the gas flow. Preliminary studies have revealed that the frequent

switching of reducing and oxidizing feed enhances the heat management inside the bed leading to more uniform solids conversions and temperature profiles [30]. Another novel configuration consists of a rotating bed that spins round while fuel and air are introduced radially. The rapid switching between the oxidation and reduction stages should prevent the development of severe temperature profiles inside the bed [31,32]. However, this reactor design entails possible gas leakages between the reaction zones and requires complex balance of plant. Finally, honeycomb-structured CLC reactors offer larger surface areas than conventional fixed-beds for an enhanced gas-solid contact. Therefore, efficient fuel conversions are feasible with higher gas velocities throughout the bed with a moderate pressure drop, which also help to maintain moderate temperature profiles inside the reactor [33].

In this short communication, we examine the basic design and performance of a new packed-bed reactor concept [34] that attempts to overcome the main limitations of previous high pressure air reactors by permitting a slow diffusional control of the solids oxidation in the air reactor.

Reactor concept and case example

The main service of a CLC power generation system is to exploit the thermal power released during the oxidation of the oxygen carrier with air. Ideally, the air reactor should be integrated within a Brayton cycle (Fig. 1, top) so that compressed air is heated up by the exothermic oxidation reaction of *Me* to *MeO* and then expanded in a turbine. The nominal inlet temperatures of modern high-efficient gas turbines are around 1400ºC, but the maximum temperatures delivered by CLC fired systems cannot exceed the 1000-1200ºC range due to the constraints imposed by the oxygen carrier properties [5, 14]. Several process schemes propose the use of an additional combustor situated downstream of the CLC reactors to heat the gas entering the gas turbine up to temperatures that would result in maximum energy conversion efficiency, at the expense of certain carbon leakage when the fuel gas contains carbon [16, 35]. The typical conditions of air fed into these CLC systems are about 500 ºC and 20 atm [26-29], so that a temperature increase in the air reactor of between 500 and 700 ºC is a reasonable compromise for design calculations. Moreover, oxidation enthalpies are very high for most oxygen

carriers (e.g. ΔH_{273K}=-553.7 kJ/molO_2 for Fe/Fe_2O_3, which is the pair of solids used in the example below). An overall heat balance in the air reactor represented in Fig. 1 (top) shows that modest conversions of O_2 in the pressurized air that lead to about 0.17-0.18 of O_2 volume fraction at the reactor exit are sufficient to heat up the circulating air to over 1100 ºC, assuming adiabatic conditions. Therefore, the main design challenge for the air reactor is to ensure a low O_2 conversion when it enters into contact with a highly reactive oxygen carrier (Me), while maintaining a reasonably low pressure drop of about 5% [26-29] in the gas subsequently expanded in the turbine for power generation. The bottom part of Fig. 1 illustrates the gas-solid contact mode adopted in the proposed air reactor to fulfill these two major constraints.

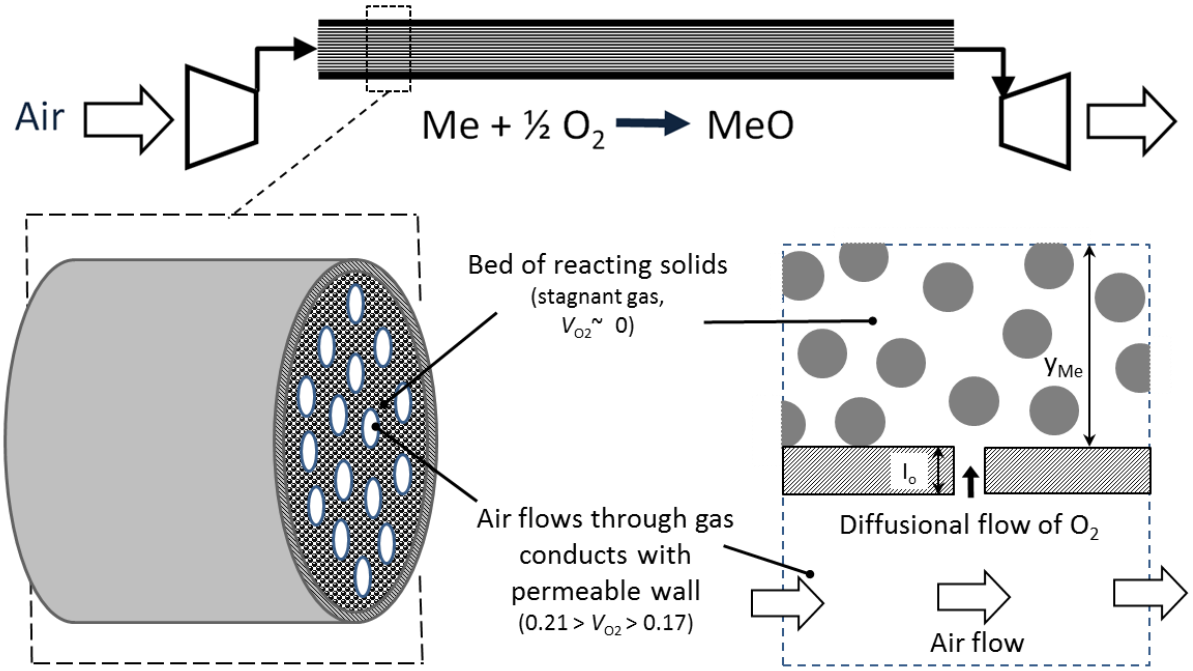

Fig. 1. Schematic representation of the novel air reactor set-up.

The overall reactor set-up is conceptually similar to that proposed by Kusano et al. in a seminal patent for the desulfurization of flue gas [36], in which a large flow of gas passes through a vessel containing bags of solid sorbent to remove SO_2. Perforated sheets or nets separate the bed of solids from the circulating gas. SO_2 then flows by diffusion through the orifices from the flue gas towards the interior of the bags, where the gas remains in a stagnant state. In the reactor proposed in this work, the same

principle is used to reduce by several orders of magnitude the oxidation rate of the oxidizing particles in the packed bed and achieve the desired modest conversion of O_2. As shown in Fig. 1, the packed bed of solids (containing the oxygen carrier in its reduced form, Me) is traversed in axial direction by conducts free of solids through which air flows at high velocity. These conducts are made of porous walls with small orifices that allow a non-selective diffusion of gas. A diffusion flow of air is established through them, perpendicular to the bulk flow of gas along the conduct. When O_2 reacts with the oxidizing solids, the heat generated is transferred through the wall of the conducts and heats up the main air stream. Despite the great reactivity of the solid particles with oxygen under CLC conditions, it is possible to impose very long oxidation times (i.e. hours), since the solids are forced to share the limited oxygen arriving from the oxygen-rich region of the air conducts. This controlled oxidation process will proceed throughout the reactor volume, thereby generating a steady axial temperature profile along the reactor without hot spots and sharp axial reaction fronts characteristic of the reactor designs mentioned above.

To illustrate with a quantitative example the viability and performance of the proposed air reactor, the basic design rules that govern the O_2 diffusional fluxes in the reactor are described below for a particular case where iron oxide (i.e. Fe/Fe_2O_3) is used as oxygen carrier.

The fraction of gas conduct wall occupied by orifices and the effective length of these orifices are critical design parameters for limiting the oxidation rate of the solids in the packed bed. The high temperature conditions existing in the air reactor will allow sufficiently fast oxidation kinetics of the oxygen carrier to ensure that the O_2 partial pressure in the voids between the particles of the packed bed remains close to zero. In these conditions, the overall reaction rate will be controlled by the flux of O_2 through the orifices of the wall ($F_{O2,}$ mol/s O_2 per m^2 of gas conduct wall), which is given by Fick´s diffusion law, according to equation (1).

$$F_{O2,z} = \frac{D_{O2,z}\ \varepsilon_w\ C_{O2,z}}{I_o} \qquad (1)$$

where D_{O2} is the local value of the diffusivity of oxygen in air, ε_w is the fraction of gas conduct wall area occupied by the orifices, $C_{O2,z}$ is the local molar concentration of O_2 and l_o is the effective length of the orifices.

The orifices are assumed to be uniformly distributed in the gas conduct wall. Their diameter should be sufficiently small to prevent the entrance of particles from the packed bed section to the air conducts and sufficiently large to reduce Knudsen diffusion effects, that would impose further limitations on the effective flux of oxygen through the wall. In steady state conditions, the initial power output from the oxidation of Me to MeO will be the local product of the flux of O_2 through the orifices and the oxidation enthalpy (i.e. $F_{O2}\cdot\Delta H_{r,O2}$), which only depends on the diffusion properties of the gas through the orifices in the wall, and not on the properties of the reacting solids or their degree of conversion.

As can be seen below, similar values of F_{O2} throughout the air reactor are feasible even with large differences in axial temperatures. This is because the fluxes of oxygen along the reactor at a given time *t* are only linked to the variability in the diffusivity and concentration of O_2 with the local operating conditions (see equation 1) once the design has been fixed (i.e. once the variables affecting the porous wall have been defined). For example, the fact that temperature has opposite effects on diffusivity and concentration of O_2 makes the oxygen fluxes to be remarkably close even at the extremely different local temperature conditions found along the reactor. In the case of pressure, this is even more pronounced as the diffusivity varies inversely proportional to pressure while concentration dependency to this variable is directly proportional. This means that O_2 fluxes, and therefore reaction rates and heat generation rates, are not affected by pressure when all other conditions are maintained. As a result, control possibilities of the oxygen fluxes for a fixed reactor design (and thus, of the thermal output) are very limited since the fluxes of oxygen barely change within the range of temperatures expected. A heat balance in an elemental volume of the reactor under adiabatic and steady state conditions allows the axial temperature profile in the reactor to be calculated by taking into account the difference in temperature between the wall ($T_{w,z}$) and air ($T_{gas,z}$), as follows:

$$\frac{d(m_{gas,z} Cp_{gas,z}\, T_{gas,z})}{dz} = A_w h_{w,z}(T_{w,z} - T_{gas,z}) = A_w F_{O_2,z}\, \Delta H_{r,O2} \quad (2)$$

where $m_{gas,z}$ is the local mass flow rate of gas, $cp_{gas,z}$ is heat capacity of the gas, A_w is the total inner area of the air conduct walls and $h_{w,z}$ is the local wall-gas heat transfer coefficient. Both temperature axial profiles $T_{w,z}$ and $T_{gas,z}$ can then be obtained from the known initial conditions at z=0 by solving equations (1) and (2).

As the particles of the oxygen carrier are progressively converted from Me to MeO, additional resistances to the reaction may appear, in addition to that of the extreme resistance imposed by the diffusion of oxygen through the porous wall. As a consequence, there may be a gradual decrease in the overall oxidation reaction rate and hence, in the power output, from a maximum value at the beginning of the operation (i.e. when the molar fraction of Me in the packed bed, X_{Me}, is equal to 1) to a minimum when the solids approach total oxidation (i.e. when X_{Me}=0 and X_{MeO}=1). In the absence of experimental information on particular materials and reactor set-ups, two extreme cases have been considered:

1. The only controlling step is the diffusion through the orifices (equation 1) and the process is not affected by the progressive conversion of the solids. This implies some kind of mass transport mechanism (for example, gas convection promoted by local temperature profiles at particle level) in the inter-particle voids of the volume associated with each orifice (represented on the right-hand side of Fig. 1). In this case, the power output will remain constant during the oxidation of the full batch of solids in the reactor and only change drastically to zero once the solids have reached full oxidation.

2. An oxidation front moves away from each orifice in perpendicular direction to the air flow in the conducts (i.e. a bed of MeO located at a distance "*y*" from the wall is growing at the expense of the initial bed of Me). In this case, the same oxygen diffusion mass balance yields Equation 3

(assuming the gas diffusivity of O_2 to be the same in the orifices and in the voids between the particles), which shows that the oxygen flux (and thus, the overall oxidation reaction rate) decreases with time as the reaction front advances in the solids bed:

$$F_{O2,z,t} = \frac{D_{O2,y,z,t}\ \varepsilon_w\ (C_{O2,z,t} - C_{O2,z,w,t})}{I_o} = \frac{D_{O2,y,z,t}\ \varepsilon_{MeO}\ C_{O2,z,w,t}}{y_{z,t}} \quad (3)$$

where $C_{O2,z,w,t}$ is the local concentration of O_2 on the side of the air conduct wall in contact with the solids bed and $y_{z,t}$ is the position of the oxidation reaction front at that point in time and reactor length. The advance of the oxidation front away from the conduct wall with time can be estimated from the overall conversion of Me to MeO ($X_{MeO,t}$) and the effective thickness of the initial packed bed of solids allocated to each air conduct (y_{Me}). Assuming Cartesian dimensions (i.e. for flat air conducts or thin packed beds per cylindrical air conduct), it can be calculated as follows:

$$y_{z,t} = X_{MeO,z,t}\ y_{Me} \quad (4)$$

As noted above, fluxes of oxygen will not change much in the axial direction, which means that an average value of $X_{MeO,t}$ can be adopted for the entire reactor at any given time. This, combined with equation (3), yields for a given time and level of conversion of the solids:

$$F_{O2,z,t} = \frac{(D_{O2,y,z,t}\ \varepsilon_w\ C_{O2,z,t})/I_o}{(1 + \frac{X_{MeO,t} y_{Me} \varepsilon_w}{I_o \varepsilon_{MeO}})} \quad (5)$$

The average conversion of the solids at any time ($X_{MeO,t}$) can be calculated from the oxygen mass balance in the solid phase associated with each orifice, which states that the oxygen that has diffused through the porous walls from time 0 to *t* must be in the form of MeO:

$$bX_{MeO,t} y_{Me} (1 - \varepsilon_{MeO}) L_r \rho_{MeO} = \int_{t=0}^{t=t} \int_{z=0}^{z=Lr} F_{O2,z,t}\, dt\, dz \quad (6)$$

where b are the moles of O_2 reacted per mol of MeO, ρ_{MeO} is the molar density of MeO (mol/m^3) and L_r is the total length of the reactor (m).

A preliminary conceptual design with Fe/Fe_2O_3 as oxygen carrier has been calculated assuming a reactor 100 m long, with an inner diameter of 2 m and traversed axially by air conducts with diameter of 0.05 m. The air reactor is able to generate a maximum power of 100 MW_{th} with the gas at the exit flowing at 1048 ºC and 18.9 atm. Dynamic temperature changes to achieve pseudo-steady states have been ignored for the sake of simplicity, because the thermal ballast associated with temperature changes in the mass of the reactor is much smaller than the total energy density stored in the reactor (3100 kWh/m^3 in the example). Moreover, no temperature profiles in the bed in a direction perpendicular to the air flow have been considered due to the modest depth of the solids bed associated with a single orifice (i.e. 0.02 m in the example). The correlations for calculating the diffusivity of oxygen and other transport properties at different temperatures have been obtained from Perry´s handbook [37]. Table 1 summarizes the reactor characteristics and the input operating conditions chosen for the case study with Fe/Fe_2O_3 and Table 2 shows the results obtained once the previous set of equations are solved.

Table 1. Reactor characteristics and operating conditions corresponding to the reference case study.

Parameters	Values
Target thermal power output (MW)	100
Reactor length, L_r (m)	100
Effective internal diameter of each air conduct, D_i (m)	0.05
Thickness or air conduct walls = diffusion length through the wall (m), l_0	0.002
Fraction of air conduct wall occupied by orifices, ε_w	0.12
Effective thickness of packed bed of iron solids around an air conduct (m), y_{Me}	0.02
Initial vol. fraction of Fe (iron sponge) in the packed bed around air conducts, $(1-\varepsilon_{Me})$	0.3
Inlet air pressure, P_{in} (atm)	20
Inlet air temperature, T_{in} (ºC)	500
Inlet air velocity in the interior of the air conduct (m/s)	20
Enthalpy of oxidation of Fe to Fe_2O_3 (kJ/mol O_2)	553.7

Maximum conversion of Fe to Fe_2O_3	1
Fe/Fe_2O_3 solid densities (kg/m^3)	7874/5250

197

198 **Table 2.** Calculated parameters at the beginning of the oxidation period in the air reactor, for the
199 operating conditions listed in Table 1 and assuming steady operation of the reactor.

Parameters	Value200
Effective total internal diameter of the reactor, (m)	1.97
Number of air conducts or pipes, N_a	438
Air conduct wall-air heat transfer coeffic., h, at reactor inlet (outlet) (W/m^2K)	480 (615)[1]
Diffusivity of O_2 in N_2, $D_{O2,z}$ at inlet (outlet) ($m^2/s \times 10^{-6}$)	5.4 (11.9)[2]
Initial flux of oxygen trough the wall, inlet (outlet) of the reactor, (mol O_2/m^2s)	0.182 (0.219)
Fanning factor at inlet	0.00545[3]
Temperature of the gas at the reactor exit, (ºC)	1048
O_2 volume fraction at the reactor exit	0.185
Gas velocity at the reactor exit, (m/s)	33.13
Pressure at the reactor exit, (atm)	18.93
Minimum time to complete the oxidation of the solids in the reactor, (hours)	9.22
Average energy density stored in the full reactor at t=0 (kWh/m^3 reactor)	3099

201 [1] $Nu=0.023 \cdot Re^{0.8}Pr^{0.4}$; [2] $D_{O2,z}=0.113 \cdot (T+273)^{1.724}/P$ ($m^2/s \times 10^{-8}$); [3] $f_F=0.04/Re^{0.16}$

202 Under these controlled oxidation conditions, and for the case 1 noted above, it would take more than
203 9 hours for the oxygen to oxidize the entire packed bed. It should be mentioned that the operation of
204 the reactor in a subsequent reduction cycle (i.e. Fe_2O_3 to Fe) involving the feeding of a fuel gas is
205 considered outside the scope of this work. In general, the operation of this fuel reactor will entail less
206 challenging reaction conditions and time scales, since fuel flow rates are typically one order of
207 magnitude lower than the air flows in the air reactors, reduction enthalpies are lower than oxidation

208 enthalpies and the operation times can also be much longer (in particular when the air reactor is used
209 only as back-up power system).

210 As mentioned above, the calculated flux of O_2 through the orifices of the wall is very similar along the
211 air reactor despite the large difference in temperatures between the inlet and outlet of the axial
212 conducts. In fact, this phenomenon makes the axial heat generation rate and temperature profiles
213 virtually linear, as can be seen in Fig. 2a (solid lines). These temperature profiles are very sensitive to
214 design decisions that determine such oxygen fluxes.

215 In addition, for the case 2 described around equation 3, additional resistances to O_2 diffusion in the
216 orifice will appear in the bed, resulting in a drop in temperatures at the reactor exit (see dotted line
217 Fig. 2a, for a constant mass flow at the inlet). In this case study, when almost all the iron present in the
218 bed has been converted into Fe_2O_3, the temperature of the gas leaving the reactor would be around
219 660 ºC.

220

221

222

223

224

225

226

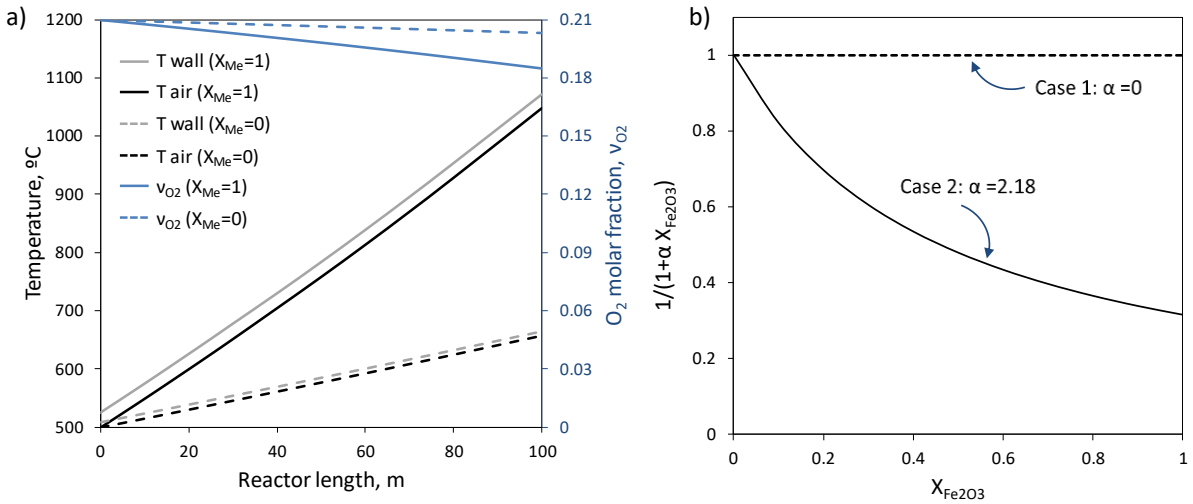

227

228 **Fig. 2.** a) Axial temperature and oxygen profiles (right axis) of air and conducts wall at the beginning of
229 the oxidation stage (solid lines) and when the solids bed is approaching full oxidation (dotted lines); b)
230 Fall in oxygen fluxes and reactor power output as a function of the conversion of Fe to Fe_2O_3 for cases
231 1 and 2 (using the data listed in Table 1 to calculate α=2.18).

232 Figure 2b shows the decay in power output during the operation under the mode described in case 2.
233 As can be seen, the term "$\alpha = y_{Me}\,\varepsilon_w / l_o\,\varepsilon_{MeO}$" in equation (5) entails critical design decisions, since the
234 fact that bringing it towards zero to maintain the production of power stable will involve much thinner
235 layers of oxygen carrier per each associated air conduct (i.e. more air conducts for a given amount of
236 solids), much longer reactors to operate with smaller fraction of air conduct wall occupied by orifices
237 (ε_w), or larger wall thicknesses with a more loosely packed bed of solids (l_o).

238 The decay in power output of the proposed air reactor due to the additional diffusional resistance as
239 the conversion of the solids progresses may be unavoidable, but this should not be a showstopper for
240 the use of this diffusion controlled reactor in applications where a steady power supply is demanded.
241 A straightforward solution to ensure steady outputs has already been mentioned above: this consists
242 in burning a minor flow of fuel gas at the reactor exit (or at turbine entrance) to top up temperatures,
243 and consequently, the efficiency of the Brayton cycle [16, 35]. Therefore, the proposed reactor could
244 be of practical use for wide range of applications, including mobile applications (e.g. boats) and other

245 systems that could accommodate high L/D aspect ratios. However, clearly more theoretical and
246 experimental work is needed to proof the concept.

247 **References**

248 [1] M. Ishida, H. Jin, A new advanced power-generation system using chemical looping combustion,
249 Energy 19 (1994) 415–422.

250 [7] A. Lyngfelt, B. Leckner, T. Mattisson, A fluidized-bed combustion process with inherent CO_2
251 separation; application of chemical-looping combustion, Chem. Eng. Sci. 56 (2001) 3101–3113.

252 [3] M. Ishida, M. Yamamoto, T. Ohba, Experimental results of chemical-looping combustion with
253 $NiO/NiAl_2O_4$ particle circulation at 1200 degrees C, Energ. Conv. Manag., 43 (2002) 1469-1478.

254 [4] O. Brandvoll, O. Bolland, Inherent CO_2 capture using chemical looping combustion in a natural gas
255 fired power cycle, J. Eng. Gas Turbines Power 126 (2004) 316–321.

256 [5] J. Adanez, A. Abad, F. Garcia-Labiano, P. Gayan, L.F. de Diego, Progress in chemical-looping
257 combustion and reforming technologies, Prog. Energy Combust. Sci. 38 (2012) 215–282.

258 [6] L.S. Fan, L. Zeng, W. Wang, S. Luo, Chemical looping processes for CO_2 capture and carbonaceous
259 fuel conversion – prospect and opportunity, Energ. Environ. Sci. 5 (2012) 7254–7280.

260 [7] A. Lyngfelt, Chemical-looping combustion of solid fuels – Status of development, App. Energ. 113
261 (2014) 1869–1873.

262 [8] S. Banerjee, R.K. Agarwal, Review of recent advances in process modeling and computational fluid
263 dynamics simulation of chemical-looping combustion, 18 (2017) 1-37.

264 [9] M Matzen, J. Pinkerton, X. Wang, Y. Demirel, Use of natural ores as oxygen carriers in chemical
265 looping combustion: A review, Int. J. Greenh. Gas Con. 65 (2017) 1-14.

266 [10] J. Adanez, A. Abad, T. Mendiara, P. Gayan, L.F. de Diego, F. Garcia-Labiano, Chemical looping
267 combustion of solid fuels, Progress in chemical-looping combustion and reforming technologies, Prog.
268 Energy Combust. Sci. 65 (2018) 6-66.

269 [11] T. Song, L. Shen, Review of reactor for chemical looping combustion of solid fuels, Int J. Greenh.
270 Gas Con. 76 (2018) 92-110.

271 [12] T. Mattisson, M. Keller, C. Linderholm, P. Moldenhauer, M. Ryden, H. Leion, A. Lyngfelt, Chemical-
272 looping technologies using circulating fluidized bed systems: Status of development, Fuel Proces.
273 Technol. 172 (2018) 1–12.

274 [13] Z. Chen, L. Qin, J.A Fan, L.S. Fan, New Insight into the Development of Oxygen Carrier Materials
275 for Chemical Looping Systems, Engineering, 4 (2018) 343-351.

276 [14] J. Hu, V.V. Galvita, H. Poelman, G.B. Marin, Advanced chemical looping materials for CO_2
277 utilization: A review, Materials, 11 (2018) 1187-1219.

278 [15] A. Lyngfelt, A. Brink, O. Langorgen, T. Mattisson, M. Ryden, C. Linderholm, 11,000 h of chemical-
279 looping combustion operation—Where are we and where do we want to go? Int. J. Greenh. Gas Con.
280 88 (2019) 38-56.

281 [16] R. Naqvi, O. Bolland, Multi-stage chemical looping combustion (CLC) for combined cycles with CO_2
282 capture. Int J Greenh. Gas Con. 1 (2007) 19–30.

283 [17] H.M. Kvamsdal, K. Jordal, O. Bolland, A quantitative comparison of gas turbine cycles with CO_2
284 capture, Energy 32 (2007) 10-24.

285 [18] R. Naqvi, J. Wolf, O. Bolland, Part-load analysis of a chemical looping combustion (CLC) combined
286 cycle with CO_2 capture, Energy 32 (2007) 360–370

287 [19] R. Xiao, Q. Song, M. Song, Z. Lu, S. Zhang, L. Shen, Pressurized chemical-looping combustion of
288 coal with an iron ore-based oxygen carrier, Combust. Flame 157 (2010) 1140-1153.

289 [20] A. Bischi, O. Langørgen, I. Saanum, J. Bakken, M. Seljeskog, M. Bysveen, J.X. Morin, O. Bolland,
290 Design study of a 150kWth double loop circulating fluidized bed reactor system for chemical looping
291 combustion with focus on industrial applicability and pressurization, Int. J. Greenh. Gas Con. 5 (2011)
292 467-474.

293 [21] S. Noorman, M. van Sint Annaland, H. Kuipers, Packed bed reactor technology for chemical-
294 looping combustion, Ind. Eng. Chem. Res. 46 (2007) 4212-4220.

295 [22] S. Noorman, F. Gallucci, M. van Sint Annaland, H. Kuipers, Experimental investigation of a
296 CuO/Al_2O_3 oxygen carrier for chemical-looping combustion. Ind. Eng. Chem. Res. 49 (2010) 9720-9728.

297 [23] S. Noorman, F. Gallucci, M. van Sint Annaland, J.A.M Kuipers, A theoretical investigation of CLC in
298 packed beds. Part 2: Reactor model. Chem. Eng. J. 167 (2011) 369-376.

299 [24] V. Dupont, A.B. Ross, E. Knight, I. Hanley, M.V. Twigg, Production of hydrogen by unmixed steam
300 reforming of methane, Chem. Eng. Sci. 63 (2008) 2966-2979.

301 [25] A. Antzara, E. Heracleous, A.A. Lemonidou, Energy efficient sorption enhanced chemical looping
302 methane reforming process for high-purity H_2 production: Experimental proof-of-concept, App. Energ.
303 180 (2016) 457-471.

304 [26] V. Spallina, F. Gallucci, M.C. Romano, P. Chiesa, G. Lozza, M. van Sint Annaland, Investigation of
305 heat management for CLC of syngas in packed bed reactors. Chem. Eng. J. 225 (2013) 174-191.

306 [27] V. Spallina, P. Chiesa, E. Martelli, F. Gallucci, M.C Romano, G. Lozza, M. van Sint Annaland,
307 *Reactor design and operation strategies for a large-scale packed-bed CLC power plant with coal*
308 *syngas.* Int. J. Greenh Gas Con. 36 (2015) 34-50.

309 [28] J.R. Fernandez, J.C. Abanades, Conceptual design of a Ni-based chemical looping combustion
310 process using fixed-beds, App. Energ. 135 (2014) 309-319.

311 [29] J.R. Fernandez, J.M. Alarcon, Chemical looping combustion process in fixed-bed reactors using
312 ilmenite as oxygen carrier: Conceptual design and operation strategy, Chem. Eng. J. 264 (2015) 797-
313 806.

314 [30] L. Han, G.M. Bollas, Chemical-looping combustion in a reverse-flow fixed bed reactor. Energy 102
315 (2016) 669–81.

316 [31] S.F. Håkonsen, R. Blom, R., Chemical looping combustion in a rotating bed reactor – Finding
317 optimal process conditions for prototype reactor. Environ. Sci. Technol. 45 (2011) 9619-9626.

318 [32] Z. Zhao, T. Chen, A.F. Ghoniem, Rotary bed reactor for chemical-looping combustion with carbon
319 capture. Part 1: reactor design and model development. Energy Fuel 27 (2012) 327–343.

320 [33] H. Zhang, H. Hong, Q. Jiang, Y. Deng, H. Jin, Q. Kang, Development of a chemical-looping
321 combustion reactor having porous honeycomb chamber and experimental validation by using
322 $NiO/NiAl_2O_4$, App. Energ. 211 (2018) 259-268.

323 [34] J.C. Abanades, Reactor for heating a gas and uses thereof, Patent Application to the European
324 Patent Office PCT/EP2019/063643, 2019.

325 [35] S. Consonni, G. Lozza, G. Pellicia, S. Rossini, F. Saviano, Chemical-looping combustion for combined
326 cycles with CO_2 capture, J. Eng. Gas Turb. Power 128 (2006) 525–534.

327 [36] K. Kusano, H. Ando, T. Kagami, A. Uchida, N. Akiyama, Y. Ueda, Y. Akiba, Apparatus for facilitating
328 contact between solid particles and fluid, Patent GB1467277A, 1974.

329 [37] R.B. Perry, D.W. Green, Perry's Chemical Engineers' Handbook, McGraw-Hill, 1999.